JOURNAL OF MATERIALS SCIENCE 14 (1979) 2605–2615

The temperature dependence of the fracture toughness and acoustic emission of polycrystalline alumina

B. J. DALGLEISH, A. FAKHR, P. L. PRATT, R. D. RAWLINGS
Department of Metallurgy and Materials Science, Imperial College of Science and Technology, London SW7 2BP, UK

The technique of acoustic emission has been shown to be suitable for the monitoring of fracture-toughness tests over a range of temperatures. Commercial polycrystalline alumina has been tested at temperatures up to 1000° C to determine the effect of microstructure and impurity content on fracture toughness and acoustic emission. For a given alumina there was no significant variation in acoustic response or fracture toughness up to 650° C. The emissions observed prior to fracture in this temperature range were attributed to subcritical crack growth. The number of emissions depended on the amount of subcritical crack growth, the grain size, and the presence and amount of porosity. Above 650° C the fracture behaviour changed due to the flow of a grain-boundary glassy phase. This was associated with a peak in the temperature dependence of the apparent K_{IC} and was accompanied by a large number of acoustic events of low amplitude and low pulse width. At these elevated temperatures the extent of grain-boundary glassy flow, and hence the acoustic response, increased with decreasing grain size and increasing impurity content.

1. Introduction

Acoustic emission is the term applied to the stress waves released as a result of dynamic processes, such as crack growth and plastic deformation, occurring within a material. Acoustic emission is, therefore, a suitable technique for the continuous monitoring of the deformation processes taking place during fracture toughness testing. This technique has been widely used in deformation studies on metals, but as yet limited information is available on the acoustic response of ceramics.

Although the room temperature fracture toughness of alumina has been extensively studied, the toughness at elevated temperatures has received little attention. Some measure of the mechanical behaviour of alumina at elevated temperatures has been obtained by means of three-point bending [1, 2] and compression testing [1, 3, 4], and some elevated temperature toughness data have been obtained by the authors [5] and by Claussen *et al.* [6]. This paper reports the results of the first detailed study of the effect of composition and microstructure on the acoustic emission and fracture toughness of alumina over the temperature range 25 to 1000° C.

2. Experimental procedure

2.1. Material

Three polycrystalline alumina samples, which were produced by isostatically cold pressing and firing on commercial schedules, were supplied by Smiths Industries Ltd (designated FAO) and by Anderman and Ryder Ltd. (designated A1 and A2). The purities quoted by the manufacturers were 95%, 97.7% and 97.5% for FAO, A1 and A2, respectively, and typical analyses are presented in Table I. The composition and the phases present in the aluminas were further assessed by X-ray fluorescence, X-ray diffraction, together with energy-dispersive X-ray analysis of second-phase particles in a scanning electron microscope.

Light microscopy was used to characterize the

0022–2461/79/112605–11 $03.10/0

TABLE I Chemical analysis of sintered aluminas

Alumina	% Impurity				Principal impurity phase
	SiO_2	MgO	CaO	TiO_2	
FAO	2.5	0.5	2.0	<0.3	$CaO6Al_2O_3$
A1, A2	1.75	0.8	0.4	–	$MgOAl_2O_3$

microstructure of the aluminas and bulk densities were calculated from mass-volume measurements of carefully machined plates.

2.2. Mechanical properties

Earlier work by the authors [5, 7] has shown that the double cantilever beam (DCB) specimen geometry is acoustically noisier than the single edge-notched beam and double torsion geometries. Consequently, double cantilever beam specimens were chosen for this investigation even though it appears from room temperature data that this geometry yields the least satisfactory fracture toughness values [8]. DCB tests were carried out at temperatures between room temperature and 1000° C.

A PZT resonant transducer was coupled to a stainless-steel wave guide which was attached to the DCB specimen with grease and held in position by asbestos string. The grease decomposed at relatively low temperatures leaving a residue which gave good acoustic coupling. The output of the transducer was amplified and monitored with standard Dunegan–Endevco acoustic emission equipment with facilities for ring-down and event counting, and for measuring amplitude and pulse width distributions. The amplitude distributions were analysed using a power law [9], namely:

$$n(a) = \left(\frac{a}{a_0}\right)^{-b}$$

where $n(a)$ is the fraction of the emission population whose peak amplitude exceeds amplitude a, a_0 is the lowest detectable amplitude, and the exponent b characterizes the amplitude distribution.

Scanning electron microscopy was used to examine fracture surfaces, the specimens being coated with a 200 Å layer of gold to prevent charging in the microscope.

3. Results

3.1. Materials characterization

The impurity levels obtained from X-ray fluorescence measurements of the aluminas confirmed the manufacturers' analyses, i.e. A1 and A2 are of approximately the same purity, whereas FAO is considerably less pure and in particular has a high level of calcium. The presence of magnesium was unconfirmed since X-ray fluorescence is insensitive to low levels of this element. However, X-ray diffraction analysis demonstrated that the principal minor phase in the A1 and A2 materials was spinel

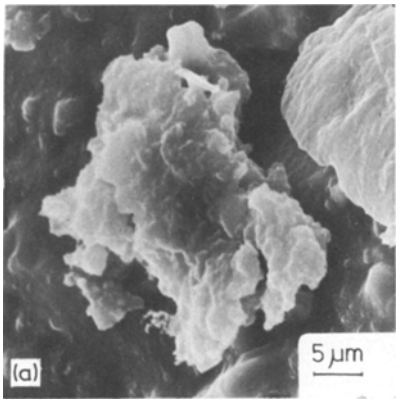

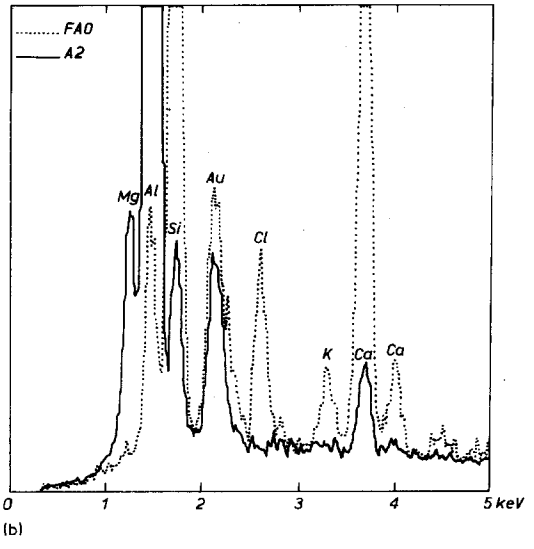

Figure 1 (a) Scanning electron micrograph of a typical second-phase particle observed in alumina FAO. (b) Energy dispersive microanalysis of second-phase particles observed in aluminas FAO and A1.

TABLE II Microstructural characteristics of the polycrystalline aluminas

Material	Density ($\times 10^3$ kg m^{-3})	Porosity (%)	Max pore size (μm)	Grain size (μm)	
				Mean	Max.
FAO	3.75	6	30	4	35
A1	3.90	1	12	2	30
A2	3.63	9	55	24	100

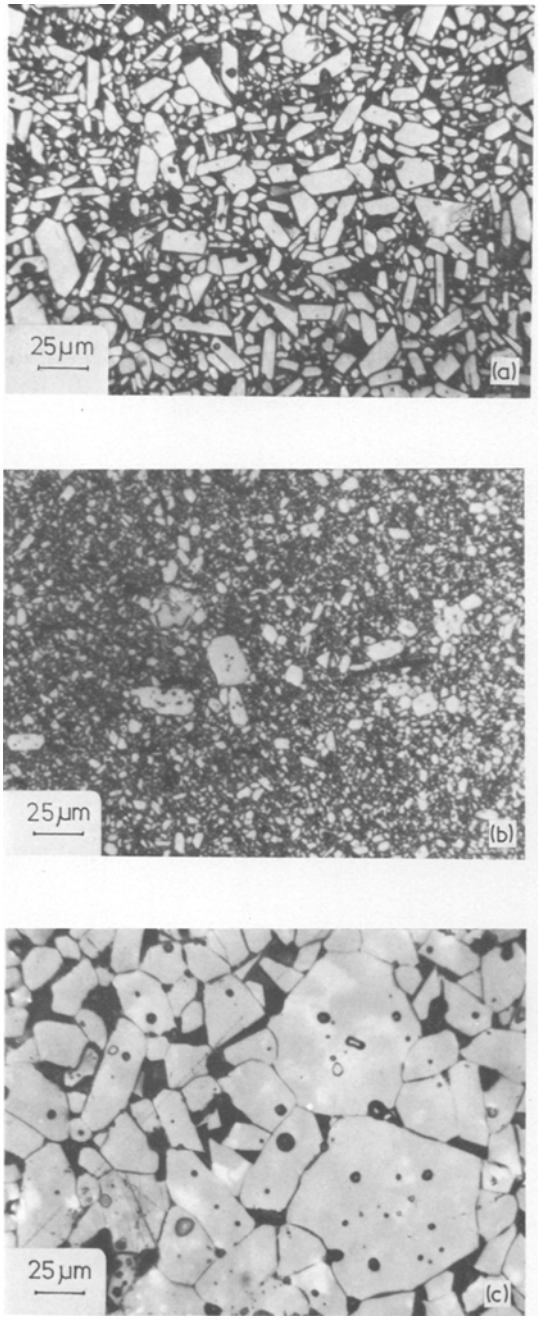

Figure 2 Optical micrographs of aluminas (a) FAO, (b) A1 and (c) A2.

($MgOAl_2O_3$). Spinel was also found in FAO, but in this material the major impurity phases were calcium based, principally calcium hexaluminate ($CaO6Al_2O_3$) and anorthite ($CaOAl_2O_32SiO_2$). Second phase particles were observed in all the aluminas, but were far more numerous in the impure alumina FAO. Fig. 1a shows a second-phase particle typical of those found on the fracture surface in FAO. Energy-dispersive analysis of the second-phase particles in room temperature fracture surfaces of FAO and A2 confirmed the increased level of calcium in the former (Fig. 1b). Finally, all three materials contained varying amounts of a glassy phase.

The essential features of the density, porosity and grain size of the aluminas are presented in Table II and Fig. 2. The microstructure of FAO consisted of a matrix of fine-grained material which contained a significant proportion of large grains up to 35 μm diameter (Fig. 2a). The porosity was mainly intergranular, rounded, and smaller than the coarse grains.

The matrix grain size of A1 was similar to that of FAO (Fig. 2b), but with a smaller proportion of the large grains. There was some angular intergranular porosity, regions of which were interconnected, but the overall porosity content was much less than that in FAO. A much larger mean grain size of 24 μm was found for alumina A2 (Fig. 2c), whilst the maximum grain size approached 100 μm. There was a large amount of angular intergranular, and rounded intragranular, porosity giving a high overall level of 9%.

3.2. Fracture toughness and acoustic emission

The load–deflection curves for a number of tests in the temperature range 25 to 1000° C for alumina A1, together with the associated acoustic response, are shown in Fig. 3. Similar curves were obtained for A2 and FAO. In all cases at temperatures below about 550° C there was a linear relationship between load and displacement up to the fracture load of P_F. However, as previously observed by

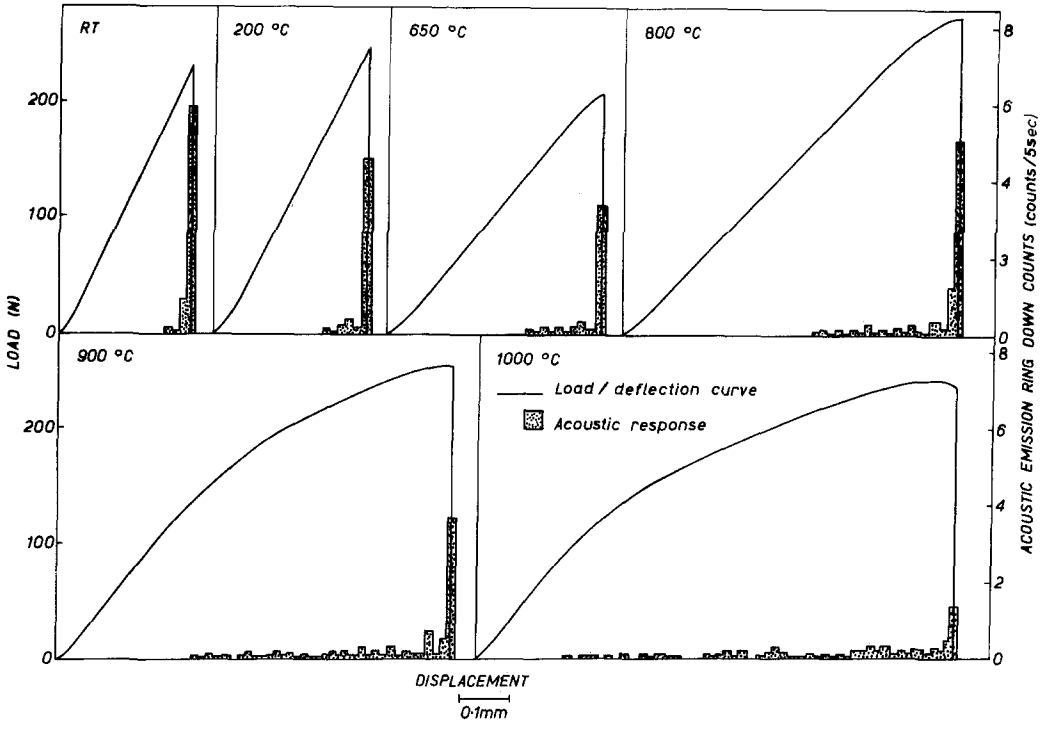

Figure 3 Load–deflection curves and acoustic response for DCB specimens of alumina A1 tested at elevated temperatures.

Fakhr *et al.* [10] for Al_2O_3, $Al_2O_3.ZrO_2$ and reconstituted brick, acoustic emission commenced at a load P_S, which was less than the fracture load.

Marked non-linearity of the load–deflection curves was observed for all the aluminas at temperatures at and above 650° C and increased with increasing temperature. At these temperatures (650 to 1000° C) acoustic emission commenced in the linear region of the load–deflection curve and continued at an increased rate through the non-linear region until fracture.

The temperature dependence of the total number of events N_{ET} for the three aluminas is shown in Fig. 4. The curves are all similar in form in that for a given material there was an approximately constant number of events up to 650° C, and thereafter the number of events dramatically increased.

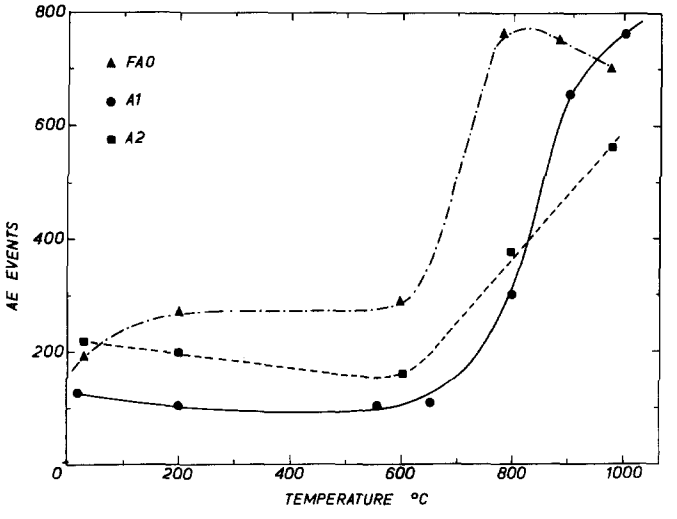

Figure 4 The temperature dependence of acoustic response of aluminas FAO, A1 and A2.

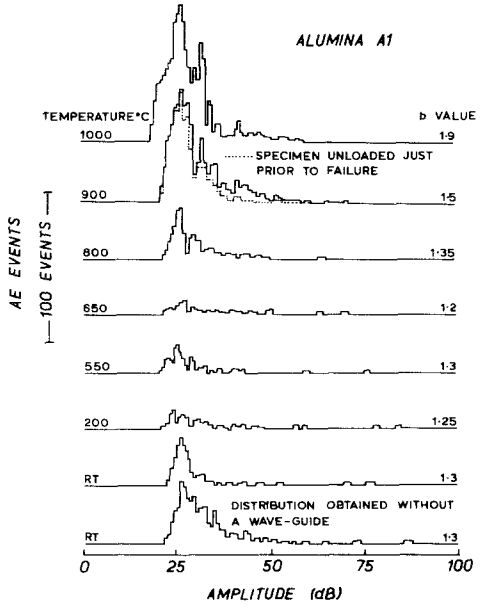

Figure 5 The acoustic emission amplitude distribution as a function of temperature. The dotted distribution at 900° C is for a test that was stopped before catastrophic failure.

The amplitude and pulse width distributions also changed in a regular manner with increasing temperature (Figs. 5 and 6). Typically above 650° C there was a marked increase in the number of low amplitude, low pulse width emissions. Two

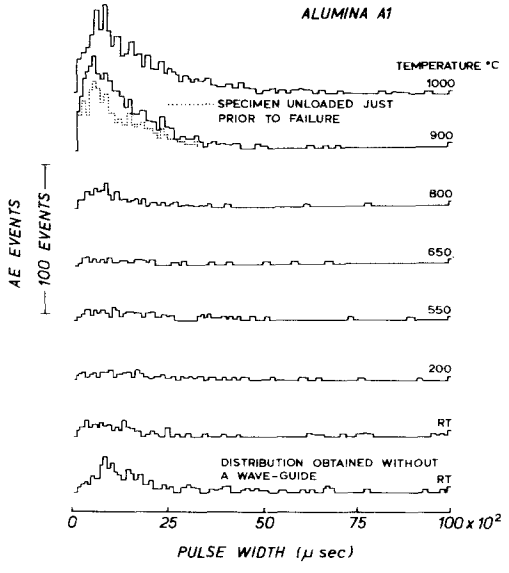

Figure 6 The acoustic emission pulse width distribution as a function of temperature. The dotted distribution at 900° C is for a test that was stopped before catastrophic failure.

further points arise from these graphs. The first concerns the detection of acoustic emission when employing a remote transducer with a wave-guide, which inevitably leads to some loss in sensitivity. It is clear from the room temperature results obtained with and without a wave-guide that, although the wave-guide reduced N_{ET}, the distributions were only marginally affected. In addition it was found that the stress P_S for the onset of emission was, within experimental error, unaltered by the use of a wave-guide. Secondly, the two amplitude distributions at 900° C, corresponding to a specimen unloaded just prior to failure and to a fractured specimen, demonstrate that most of the emissions occurred prior to failure and those associated with final fracture tended to be of high amplitude.

The apparent fracture toughness was determined from the fracture load P_F using the equation:

$$K_{IC} = \frac{P_F a_0}{b_n h^{3/2}} \left[3.467 + 2.315\left(\frac{h}{a_0}\right)\right]\left(\frac{b_n}{b_0}\right)^{1/2}, \quad (1)$$

where a_0 is the initial crack length, b_n is the crack plane width, b_0 is the plate thickness, h is the beam half-height, and the factor $(b_n/b_0)^{1/2}$ accounts for the effect of side-grooving.

The temperature dependence of the apparent fracture toughness is given in Fig. 7. Although the absolute values for the fracture toughness of the three aluminas differed, the temperature dependence in each case exhibited the same features, i.e. K_{IC} was approximately constant up to 600° C and then increased to a maximum at 750 to 850° C. Very similar temperature dependencies, with peaks at elevated temperatures, have been reported for the fracture strength in three-point bending of commercial aluminas [1], and for the fracture toughness of impure, low-density alumina [6].

4. Discussion

The main features of the temperature dependence of the acoustic emission and of the fracture toughness of the three aluminas are similar, and differ only in detail. In particular, it is clear that in all cases there was a change in deformation mechanism at approximately 650° C and, consequently, the results will be discussed in two sections corresponding to the temperature ranges 25 to 650° C and 650 to 1000° C.

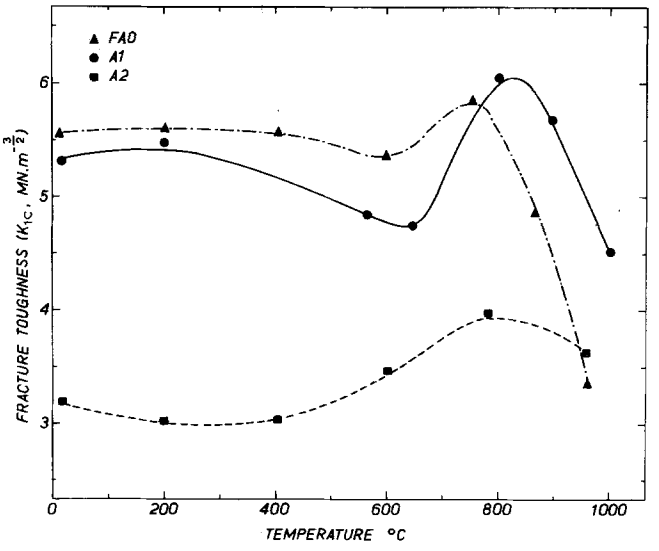

Figure 7 The temperature dependence of the apparent fracture toughness of aluminas FAO, A1 and A2.

4.1. Properties in the temperature range 25 to 650° C

The acoustic emission of aluminas during fracture testing at room temperature has been extensively investigated [8]. It was found that for testing conditions that resulted in linear load–deflection curves, approximately 80% of the total number of acoustic events monitored during a test were associated with sub-critical crack growth and the remaining events with the final fracture process. Furthermore, quantitative relationships between acoustic emission and sub-critical crack growth were determined so enabling the true crack length at failure to be substituted for a_0 in Equation 1 in order to obtain valid K_{IC} values.

The similarity of the acoustic response in all the low temperature tests, e.g. a small number of events, and the b-exponent in the range 1.0 to 1.4, indicates that sub-critical crack growth occurred at all temperatures up to 650° C. It follows that the low temperature K_{IC} values of Fig. 7 should be corrected for sub-critical crack growth. The corrected K_{IC} values shown in Fig. 8 were calculated assuming the room temperature correction procedure was applicable up to 650° C. The relative magnitudes of the fracture toughness of the three aluminas are but little altered by the correction procedure and it can be seen that A2 has a poor resistance to fracture compared with A1 and FAO.

The fracture mode of each of the materials was predominantly intercrystalline over this temperature range although some regions of cleavage were

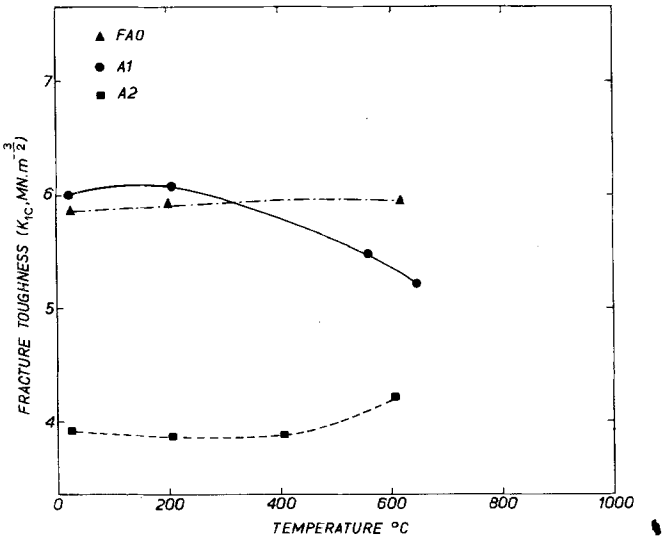

Figure 8 Fracture toughness values after correction for sub-critical crack growth.

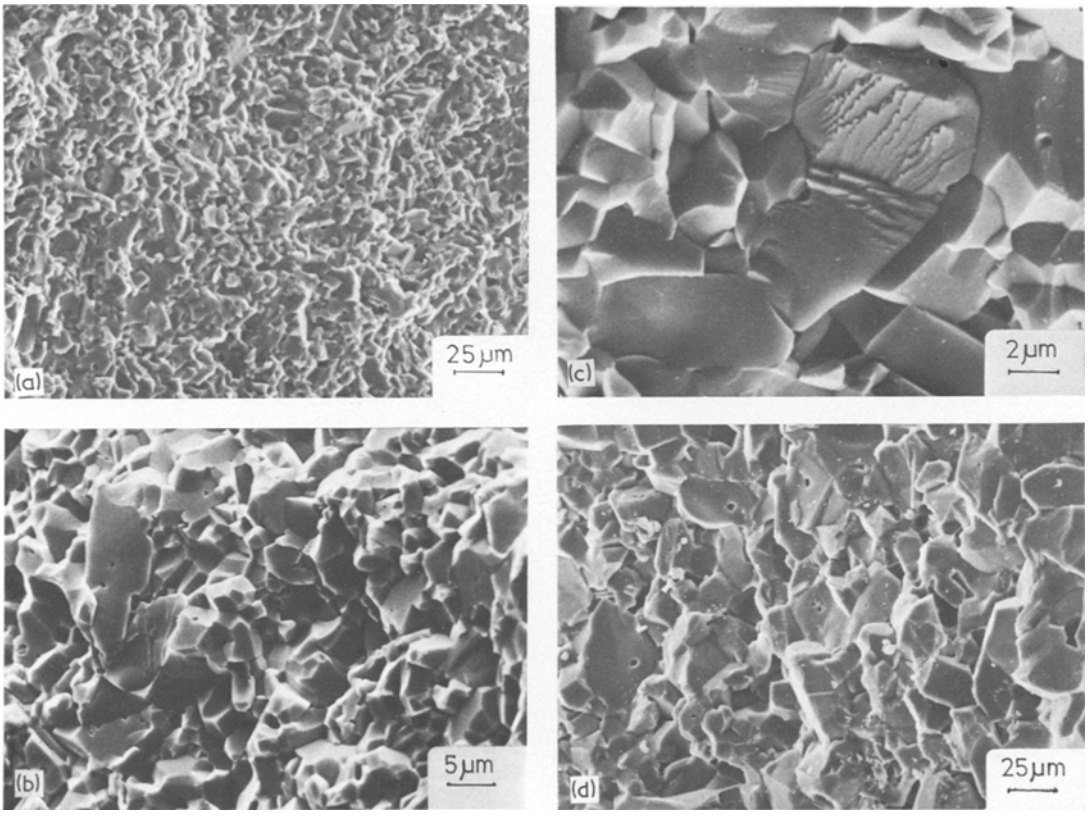

Figure 9 (a) FAO tested at room temperature. Although the fracture is intercrystalline the surface is flatter and less angular, due to the glassy phase, than that of A1 and A2. (b) A1 tested at room temperature. The intercrystalline nature of the fracture is apparent, with angular porosity. (c) A1 tested at 550° C. A region of cleavage is shown in the centre of the micrograph. (d) A2 tested at room temperature. The fracture is intercrystalline; angular intergranular porosity and grain-boundary debris can also be seen.

observed in A1 at 550° C and at 650° C. This is illustrated in the scanning electron micrographs of Fig. 9, which show the low temperature fracture surfaces of FAO, A1 and A2. By comparing with Fig. 1a, the second-phase particles in FAO can be identified fairly readily in Fig. 9a. In all cases the particles appear to have separated from the surrounding grains and thus to be non-coherent. The porosity is rounded rather than angular, as seen already in Fig. 2a. For A1, Fig. 9b confirms the angular nature of the much reduced porosity seen in Fig. 2b, while Fig. 9c shows this angular porosity at higher magnification, together with transgranular cleavage fractures at 550° C. The large angular porosity in A2, shown so clearly in Fig. 2c, can be recognized on the fracture surface in Fig. 9d.

Twinning has been reported by Lankford [2, 4] in room temperature compression and bending tests but scanning electron microscopy of the sub-critical crack, and catastrophic crack, fracture surfaces revealed no clear evidence of this mode of deformation.

For these three aluminas, the shape, the amount and the distribution of the porosity appear to control the fracture toughness. Rice and Freiman [11] have pointed out that for intergranular fracture through intergranular pores, the fracture toughness, γ, should decrease with increasing porosity P, as:

$$\gamma = \gamma_0 e^{-cP},$$

where $\gamma_0 = \gamma$ at $P = 0$ and c is a constant between 2 and 20 that depends sensitively on the shape, orientation and packing of the voids. Now K is $= (2E\gamma)^{1/2}$ where E is Young's modulus and, for porous materials, $E = E_0 e^{-cP}$. Thus $K = K_0 e^{-cP}$, and values for c and K_0 have been calculated from the data for A1 and A2. These are given in Table III. The value of $c = 5.6$ for the Anderman and

TABLE III Room temperature fracture toughness and porosity

Material	K_{IC}(MN m$^{-3/2}$)	P	c
A1	6.1	0.01	5.6
A2	3.9	0.09	5.6
K_0	6.5	0.00	5.6
FAO	5.8	0.06	1.8

Ryder material, A1 and A2, is consistent with angular pores in the form of cubes on edge or on corner in relation to the maximum principal stress, and close to the value of 5.5 ± 0.8 found by Rice [12] from an analysis of the data of Claussen [6] for a variety of commercial aluminas. The value of $K_0 = 6.5\,\mathrm{MN\,m^{-3/2}}$ is somewhat larger than the highest reliable DCB value for this material. Using this value of K_0 for want of a better, an estimate of c for the impure alumina FAO has been made (Table III). This value of $c = 1.8$ for FAO is consistent with a model of intergranular spherical pores stacked in a staggered manner, and compares well with the value of 2.2 ± 0.1 found by Evans and Tappin [13] for approximately spherical pores. On this basis the increased grain size of A2 compared with A1 appears to have little effect on the fracture toughness, as we should expect, [6, 14, 15], and the non-coherent precipitates in FAO are too far apart to have any substantial effect either. The cross-over between A1 and FAO for corrected fracture toughness in Fig. 8 coincides with the appearance of cleavage fracture in A1 at the two higher temperatures, suggesting that the change in fracture mode is responsible in some way for the decrease in A1.

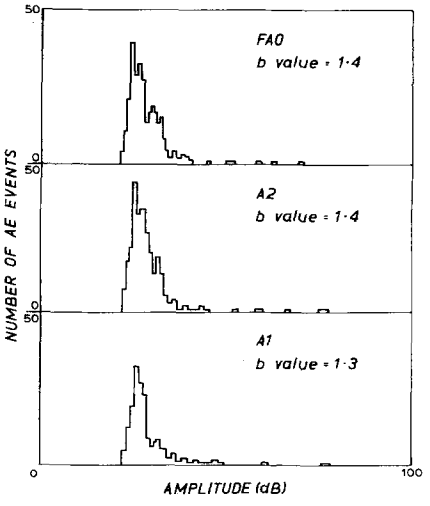

Figure 10 The room temperature acoustic emission amplitude distributions for aluminas FAO, A1 and A2.

As shown in Fig. 4, and the room temperature amplitude distribution curves of Fig. 10, the acoustic response of alumina A2 is greater than that of the fine-grained material A1. This is consistent with the observation of increasing subcritical crack growth with increasing grain size and increasing number of events per unit area of fracture surface with increasing porosity [7, 8]. The impure FAO showed a slightly greater acoustic response compared with alumina A1, in keeping with its intermediate level of porosity.

4.2. Properties in the temperature range 650 to 1000° C

In this temperature range there was a change in deformation mechanism since at these higher temperatures there was a greater proportion of low amplitude events (therefore higher b-values) and low pulse width events, and a much larger total number of events. The new deformation mechanism also resulted in a break-down in linearity of the load–deflection curves and a peak in the temperature dependence of the apparent fracture toughness.

The scanning electron micrographs of Fig. 11 are from the fracture surfaces of specimens tested at elevated temperatures. They show that fracture took place predominantly by separation at the grain boundaries and that there was a negligible amount of cleavage. In the case of alumina FAO (Fig. 11a) the surface features at low magnification appear much the same as those at low temperature, but at high magnification the glazed nature of the grain surfaces can be seen (Fig. 11b). Flow of the glassy phase in this material (Fig. 11c) is observed at 650° C. These observations are consistent with grain-boundary deformation due to flow of a glassy phase and would account for the peak in the temperature dependence of the fracture toughness. The onset of flow first led to an increase in K_{IC} as stresses were relieved at the crack tip. However, at higher temperatures (> 800° C) K_{IC} decreased as the viscosity of the glassy phase fell rapidly, facilitating easy separation of the grain boundaries. This fall-off in strength occurred at a lower temperature for the FAO alumina because of the reduced viscosity of the high calcium-content glasses believed to be present in this material. In alumina A1, even at 1000° C (Fig. 11d), there is not enough glass to round off the surface features significantly.

Comparison of the amplitude distributions at

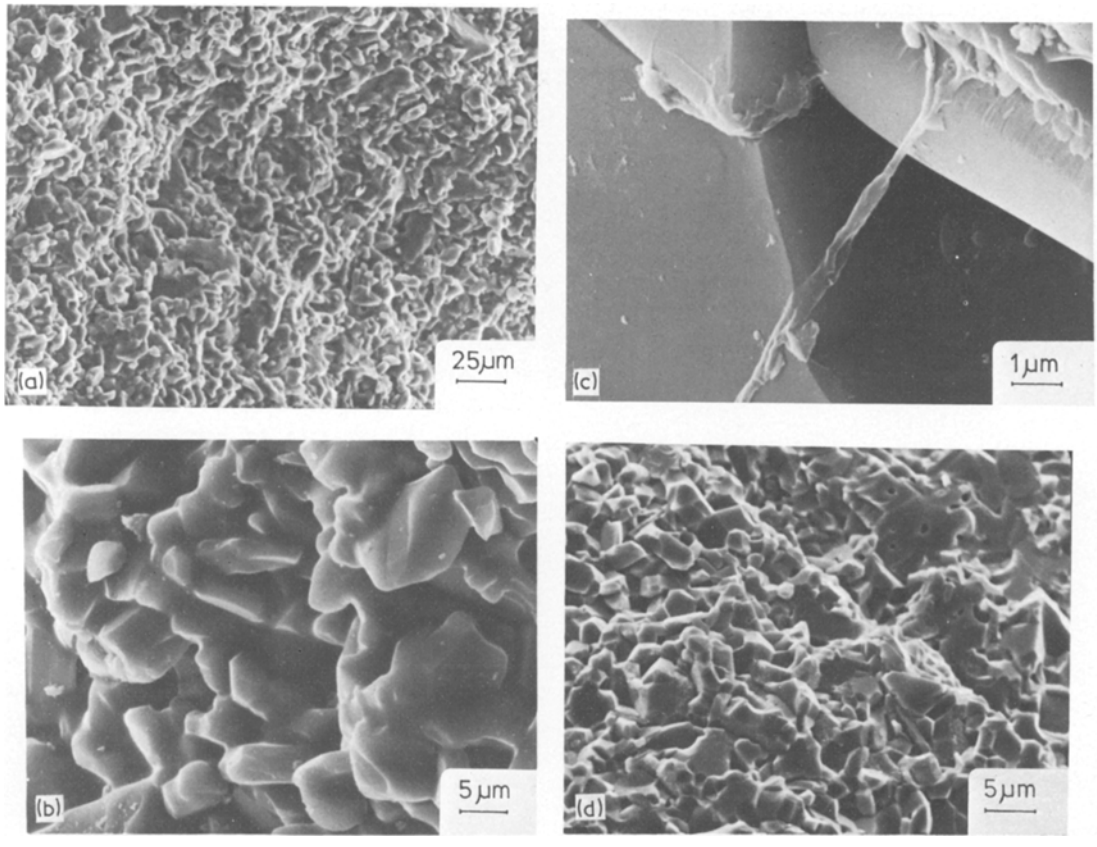

Figure 11 (a) FAO tested at 900° C. The surface is similar to that in Fig. 9a. (b) FAO tested at 900° C. The glazed nature of the grain surfaces is evident. (c) FAO tested at 650° C. Flow of the glassy phase. (d) A1 tested at 1000° C. The angular features of the grains are still visible.

900° C (Fig. 5), for fractured and unfractured specimens, demonstrates that most of the low amplitude events were associated with the grain-boundary flow and that the high amplitude events were the result of catastrophic failure. A similar, but not so clearly defined trend, is shown in the pulse width distributions (Fig. 6). It follows that the amplitude distributions at low amplitude should give an indication of the extent of the glassy flow. Indeed, it can be seen that the only difference in the amplitude distributions for the three aluminas at 900° C is in the number of low amplitude events (Fig. 12) with FAO > A1 > A2. The small-grained, impure alumina FAO contains the greatest proportion of grain-boundary glassy phase, and hence the more significant should be the grain-boundary flow. This is consistent with the acoustic emission, as the greatest number of low amplitude events was recorded for this material. Materials A1 and A2 were of similar purity but differed in grain size and percentage porosity. As in the low-temperature region, the low fracture toughness of A2 was due mainly to the high porosity content. However, the extent of glassy flow is more likely to be affected by grain size than by the presence of porosity. The large-grained alumina A2, had a reduced grain-boundary surface area and consequently should have exhibited less glassy flow. The acoustic emission data support this argument in that there was a smaller number of low amplitude emissions for A2 than A1, the reverse of the situation at room temperature.

5. The control of toughness by control of microstructure

The relationships between acoustic emission, microstructure and fracture toughness discussed in the previous section suggest ways in which the structure might be optimized for particular combinations of strength and toughness. The findings must be regarded as somewhat tentative in view of the limited range of materials and of porosities studied here, but some general principles appear to emerge, confirming that control of porosity is an

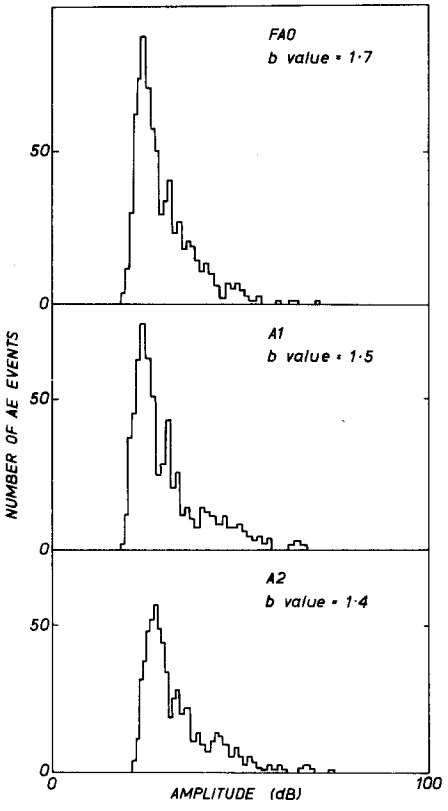

Figure 12 The acoustic emission amplitude distribution at 900° C for aluminas FAO, A1 and A2.

important factor for sintered material. The relationship $K = K_0 e^{-cP}$ shows how sensitively the corrected fracture toughness depends upon the two factors, amount and shape of porosity, in a complementary manner. The assumption in using this expression is that K is directly proportional to the minimum solid area between pores, since that is the likely path for fracture to follow. Porosity can be tolerated provided that c is kept small, for example by rounding the pores with a glassy phase that wets the grains. The best toughness results from a small number of rounded pores, and the worst from a large number of angular extended pores. Extrapolation to zero porosity is unlikely to show good agreement with experimental results for hot-pressed alumina in view of the problem of absorbed gases on the powders, as Simpson and Merrett have shown [16]. While the deliberate addition of a glassy phase appears to be helpful at room temperature in improving the corrected fracture toughness of FAO, it is clearly harmful at high temperatures. For FAO, the fall-off in strength and toughness above 650° C occurs at a lower temperature and is more marked than for the purer aluminas A1 and A2.

6. Conclusions

(1) Acoustic emission has been used successfully to monitor double cantilever beam fracture toughness tests up to 1000° C.

(2) In each of the aluminas tested the acoustic emission and the fracture toughness varied very little up to 650° C. The acoustic emission monitored prior to fracture was attributed to subcritical crack growth. In this temperature range (25° to 650° C) the fracture toughness was mainly determined by the presence of porosity and by its morphology.

(3) Above 650° C grain-boundary flow occurred which was associated with a glassy phase. This flow resulted in a peak in the temperature dependence of the apparent K_{IC} and was accompanied by a large number of acoustic events of low amplitude and low pulse width. The extent of the glassy flow and the acoustic emission increased with increasing impurity content and decreasing grain size.

Acknowledgements

The authors would like to thank Professor J. G. Ball for the provision of research facilities in the Department of Metallurgy and Materials Science, Smiths Industries and Anderman and Ryder Ltd for the provision of the polycrystalline alumina, Mr H. Haddow and Mr L. Dutton for assistance with the experimental work, and the Science Research Council and the Atomic Energy Organisation of Iran for financial support.

References

1. H. MEREDITH, C. W. A. NEWEY and P. L. PRATT, *Proc. Brit. Ceram. Soc.* **20** (1972) 299.
2. J. LANKFORD, *J. Mater. Sci.* **13** (1978) 351.
3. K. RYSHKEWITCH, *Ber. Dt. Keram. Ges.* **22** (1941) 54.
4. J. LANKFORD, *J. Mater. Sci.* **12** (1977) 791.
5. B. J. DALGLEISH, A. FAKHR, P. L. PRATT and R. D. RAWLINGS, *Ber. Dt. Keram. Ges.* **55** (1978) 511.
6. N. CLAUSSEN, R. PABST and C. P. LAHMANN, *Proc. Brit. Ceram. Soc.* **25** (1975) 139.
7. B. J. DALGLEISH, A. FAKHR, P. L. PRATT and R. D. RAWLINGS, "Physical and Metallurgical Aspects of Acoustic Emission", (Institute of Acoustics, London, 1977).
8. *Idem, Mater. Sci. Eng.* (submitted).
9. A. A. POLLOCK, *Acoustic Emission 2, Non-Destructive Testing* **6** (5) (1973) 223.

10. A. FAKHR, J. E. FREYRE and R. D. RAWLINGS, *Proc. Inst. Acoustics* 4 (1976) 1.
11. R. W. RICE and S. W. FREIMAN, presented at the "Sixth International Materials Symposium: Ceramic Microstructures" (Wiley, New York, 1976).
12. R. W. RICE, "Treatise on Materials Science and Technology", Vol. II, "Properties and Microstructure" (Academic Press, New York, 1977).
13. A. G. EVANS and G. TAPPIN, *Proc. Brit. Ceram. Soc.* **20** (1972) 275.
14. B. J. DALGLEISH, P. L. PRATT and J. SANDFORD, *Sci. Ceramics* 8 (1976) 225.
15. P. L. PRATT, "Fracture", Vol. 3 (University of Waterloo Press, Waterloo, 1977) p. 909.
16. L. A. SIMPSON and G. J. MERRETT, *J. Mater. Sci.* 9 (1974) 685.

Received 31 January and accepted 10 May 1979.